J. Astrophys. Astr. (2016) 37: 14

Large Scale Earth's Bow Shock with Northern IMF as Simulated by PIC Code in Parallel with MHD Model

Suleiman Baraka[1,2,3]

[1]*National Institute of Aerospace, 100, Exploration Way, Hampton, Virginia, USA.*
[2]*Center for Astronomy and Space Sciences-CASSR, Al Aqsa University, P.O.Box 4051, Gaza, Palestine.*
[3]*Institut d'Astrophysique de Paris, 98 bis Blvd Arago, 75015, Paris, France.*
e-mail: suleiman.baraka@gmail.com

Received 11 January 2016; accepted 8 March 2016
DOI: 10.1007/s12036-016-9389-6

Abstract. In this paper, we propose a 3D kinetic model (particle-in-cell, PIC) for the description of the large scale Earth's bow shock. The proposed version is stable and does not require huge or extensive computer resources. Because PIC simulations work with scaled plasma and field parameters, we also propose to validate our code by comparing its results with the available MHD simulations under same scaled solar wind (SW) and (IMF) conditions. We report new results from the two models. In both codes the Earth's bow shock position is found to be $\approx 14.8 R_{\rm E}$ along the Sun–Earth line, and $\approx 29 R_{\rm E}$ on the dusk side. Those findings are consistent with past *in situ* observations. Both simulations reproduce the theoretical jump conditions at the shock. However, the PIC code density and temperature distributions are inflated and slightly shifted sunward when compared to the MHD results. Kinetic electron motions and reflected ions upstream may cause this sunward shift. Species distributions in the foreshock region are depicted within the transition of the shock (measured $\approx 2c/\omega_{pi}$ for $\Theta_{Bn} = 90^{\circ}$ and $M_{\rm MS} = 4.7$) and in the downstream. The size of the foot jump in the magnetic field at the shock is measured to be $(1.7c/\omega_{pi})$. In the foreshocked region, the thermal velocity is found equal to 213 km s^{-1} at $15 R_{\rm E}$ and is equal to 63 km s^{-1} at 12 $R_{\rm E}$ (magnetosheath region). Despite the large cell size of the current version of the PIC code, it is powerful to retain macrostructure of planets magnetospheres in very short time, thus it can be used for pedagogical test purposes. It is also likely complementary with MHD to deepen our understanding of the large scale magnetosphere.

Key words. Magnetosphere—magnetopause—bow shock—PIC code—MHD model.

1. Introduction

Shocks in astrophysical systems are mainly non-relativistic shocks (relativistic shocks are not in the reach of man-made spacecraft). They have widths of order of the ion inertial length (c/ω_{pi}) or ion gyro-radius ($v_{\perp}/\omega_{ci}$ i.e. resistive scale $\sim 10^{-6}$ mean free path). The collisionless astrophysical shocks are important to understand their effects in dissipating flow-energy, in heating matter, in accelerating particles to high, presumably cosmic-ray energies, and in generating detectable radiation from radio to X-rays (Bykov & Treumann 2011; Treumann 2009).

The Earth's bow shock was proposed by Axford (1962) and Kellogg (1962). Since then many theoretical and statistical studies based on space observations have been conducted to study its position and shape for a large set of upstream solar wind plasma and field conditions (Dmitriev *et al.* 2003; Keika *et al.* 2009; Maynard *et al.* 2011; Fontaine *et al.* 2015; Jelínek *et al.* 2010; Mann *et al.* 2008; Meziane *et al.* 2015; Petrukovich *et al.* 2015). On the other hand , there are many approaches to study the bow shock location, dynamics and physical properties, such as hybrid models (Omidi *et al.* 2013; Rojas-Castillo *et al.* 2013; Ellison *et al.* 1993), MHD models (Samsonov 2007; Shaikhislamov *et al.* 2011; Kowal *et al.* 2011; Welling *et al.* 2013), and PIC models (Baraka & Ben-Jaffel 2007; Savoini *et al.* 2013; Vapirev *et al.* 2013; Schreiner & Spanier 2014) and references therein.

Leboeuf *et al.* (1978) was the first to use MHD modeling of the global interaction of the magnetosphere with the solar wind. Over the years, the scope of these models have increased and has become more sophisticated (Gombosi *et al.* 2000). The MHD use only ensemble-averaged parameters which assume the distribution of the particles velocity as a collection of several Maxwellian functions as in Winglee *et al.* (2005). Under the influence of the magnetic field where velocity distributions along and across the field lines are generally different, these calculations do not determine the plasma microphysics (Paschmann *et al.* 1981; Bonifazi & Moreno 1981; Meziane *et al.* 2007; Seki *et al.* 2009; Kronberg *et al.* 2011). On the other hand , the ideal MHD theory may eliminate the capability for the plasma to act electromagnetically. This restriction severely limits the kind of physics one can do with ideal fluid (Parks 2004).

Our code (modified from Buneman *et al.* (1992)) is a PIC code. Global PIC EM code has severe constraints on spatial and temporal scales despite containing more physics than explicitly assuming Ohm's law. The most limiting of them are $\Delta x < \lambda_{\mathrm{De}}$, $c\Delta t < \Delta x/\sqrt{n}$ and $\omega_{pe}\Delta t < 2$, where Δx is the grid size, Δt is the time step and ω_{pe} is the electron plasma frequency. However, this method is superior to MHD simulation in some aspects such as in modeling kinetic processes that separate the electrons and ions dynamics (Nishikawa 1997; Wodnicka 2009; Cai *et al.* 2006). For instance, MHD has no fundamental length scale in contrast with PIC simulations for which a gyro-radius can be derived for particles despite the limitation on the mi/me mass ratio.

In this paper, a particle-in-cell (PIC) is used for the description of Earth's bow shock. The proposed version is stable and does not require huge or expensive computer resources since we are interested in the large scales of the system ($1R_{\mathrm{E}}$) (Baraka & Ben-Jaffel 2011). The scaled plasma and field parameters used in PIC were also used to validate our code with available MHD simulations.

2. Simulation models

In this section a brief introduction of PIC-EM and MHD-GUMICS models is presented. As in our previous work (Baraka & Ben-Jaffel 2011) , the current version of the code is capable to form the macrostructure of the Earth's magnetosphere. The MHD model is introduced based on the CCMC requested run (http://ccmc.gsfc.nasa.gov/results/viewrun.php?domain=GM&runnumber=Suleiman_Baraka_112610_2). GUMICS-v4 details are also available at Janhunen *et al.* (2012).

2.1 *PIC EM relativistic global code*

In our simulation, we use the same initial conditions as in Buneman *et al.* (1980, 1992, 1995) and Buneman (1993) to generate the macrostructure of the magnetosphere. The radiating boundary conditions are adopted as in Lindman (1975) and for the charge description inside the box, we used the charge-conserving formulas reported by Villasenor & Buneman (1992). The same initial and boundary conditions were also used in our previous work (Baraka & Ben-Jaffel 2007, 2011; Baraka & Jaffel 2014; Baraka *et al.* 2013; Ben-Jaffel & Ballester 2014; Ben-Jaffel *et al.* 2013). The grid size in the simulation should take into account the nonphysical instabilities. In our simulation, they are taken care of by Courant condition ($\delta x, \delta y, \delta z > c\delta t$), which satisfies the inequality $\frac{\lambda_{\mathrm{De},i}}{\delta x} > \frac{1}{\pi}$ (Birdsall & Langdon 2005).

Pritchett (2000) thoroughly discussed the pros and cons of formulating PIC codes for space simulation. Whilst Parks (2004) clearly stated that understanding collisionless plasma dynamics requires self-consistent particle-in-cell kinetic modeling, the spatial dimensions of the 3D EM global code used in this simulation is set such that OX is pointing from Earth to Sun, OY towards dusk direction and OZ towards north direction. The dimension of the simulation box is taken equal to ($155\Delta \times 105\Delta \times 105\Delta$), where the grid size $\Delta = \Delta x = \Delta y = \Delta z = 1R_{\mathrm{E}}$ and Δt is the time step ($\omega_{pe}\Delta t = 0.22$). The simulation box is uniformly filled up by 2×10^6 of equal electron–ion pairs, this number is equivalent to a uniform particle density of $n_e = n_i = \frac{N}{\Delta^3} = 0.8$ pairs per cell.

The physical parameters (normalized) used in our simulation as pairs of numbers (unit-less values for electrons and ions) are as follows: the gyro-frequencies are $\tilde{\omega}_{ce,i} = \omega_{ce,i}\Delta t = (0.2, 0.0125)$, the thermal velocities for the two species are $\tilde{v}_{\mathrm{the},i} = v_{\mathrm{the},i}/(\Delta/\Delta t) = (0.1, 0.025) = (B\Delta m_e/\Delta t m_{e,i})$, the Debye length is $\lambda_{\mathrm{De},i} = \tilde{v}_{\mathrm{the},i}/\tilde{\omega}_{pe,i} = (0.11, 0.11)$, Larmour gyro-radii are $\tilde{\rho}_{ce,i} = \tilde{v}_{\mathrm{the},i}/\tilde{\omega}_{ce,i} = (1.25, 20)$, inertial lengths are $\tilde{\lambda}_{e,i} = \tilde{c}/\tilde{\omega}_{pe,i} = (0.559, 2.236)$. The impinged drift velocity of the solar wind along the Sun–Earth line is $V_{sw} = -0.25 = 0.5\tilde{c}$, where the speed of light's normalized value is taken as $\tilde{c} = 0.5$, the ion to mass ratio is $m_i/m_e = 16$. The normalized magnetic field is $\tilde{B} = \mathbf{B}(\frac{q(\Delta t)^2}{m_e\Delta})$, the IMF is northward $B_z(x) = 0.2$, the $\beta_{e,i} = (1.6, 6.4)$. The normalized ion temperature is $\tilde{T}_i = \tilde{v}^2_{\mathrm{the},i} m_i = 0.04$, and for electrons the temperature is $\tilde{T}_e = \tilde{v}^2_{\mathrm{the},e} m_e = 0.01$, where the '$e$' and '$i$' denote electrons and ions respectively . On the other hand , our code was run until it reached a steady state at a time step 900 Δt, where Δt is the numerical time step (Baraka & Ben-Jaffel 2011; Baraka 2007). Moreover in the PIC simulation, the macroscopic bulk properties of the flow are $V_A = 0.027$, $\frac{\mathrm{V}_A}{\mathrm{V}_{sw}} = 0.11$, $M_A = 9.219$, $M_S = 2.858$ and $M_{\mathrm{MS}} = 2.730$. Plasma parameters were then derived

and scaled so that the flow input conditions are used to simulate the same case study by MHD model.

2.2 *MHD model: GUMICS*

The Community Coordinated Modeling Center (CCMC) is a multi-agency partnership. The CCMC provides, to the international research community, access to modern space science simulations. In addition, the CCMC supports the transition to space weather operations of modern space research models. More information about CCMC can be found here (http://ccmc.gsfc.nasa.gov/).

GUMICS is a global solar wind magnetosphere–ionosphere coupling model. Its solar wind and magnetospheric part is based on solving the ideal MHD equations and its ionosphere part is based on solving the electrostatic current continuity equation. Advanced numerical methods such as automatically refined Cartesian octogrid and temporal sub-cycling are used to speed up the computation. The computational box dimension is taken from -224 to $+32R_{\mathrm{E}}$ in GSE co-ordinate X and from -64 to $+64R_{\mathrm{E}}$ in GSE co-ordinates Y and Z (Kullen *et al.* 2004; Palmroth *et al.* 2002, 2005). The official website is http://ccmc.gsfc.nasa.gov/models/modelinfo.php?model=GUMICS.

The inflow boundary conditions are carried out in 5 h, and the dipole tilt in GSE coordinates is taken to be zero. The initial solar wind velocity is $V_{sw}(x) = -500$ km s^{-1}, the solar wind density is $\rho_{sw} = 5.0$ N cm^{-3}. The solar wind temperature is $T_{e,i} = 6.7 \times 10^5$ K. The initial IMF value in the MHD code was $B_z = 6.5$ nT northward oriented. The top level (in terms of hierarchy) of the simulation box has a base grid of $(8R_{\mathrm{E}})^3$. Each cell is broken into 8 sub cells if the refinement exceed a certain limit. The grid size in the magnetohydrodynamics code is changing with the dynamics of the hierarchically adaptive and can reach up to $0.25R_{\mathrm{E}}$ (Janhunen *et al.* 2012).

3. Results

The large scale Earth's magnetosphere is simulated by PIC EM relativistic code in parallel with MHD code. One of the key features of both runs is the structure,

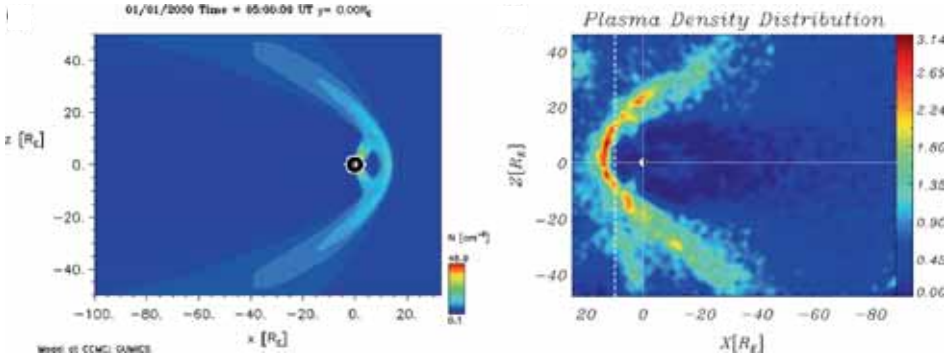

Figure 1. Plasma density distribution in noon–midnight axis. (**a**) The MHD system generated plasma distribution, (**b**) the plasma distribution as simulated by the PIC code.

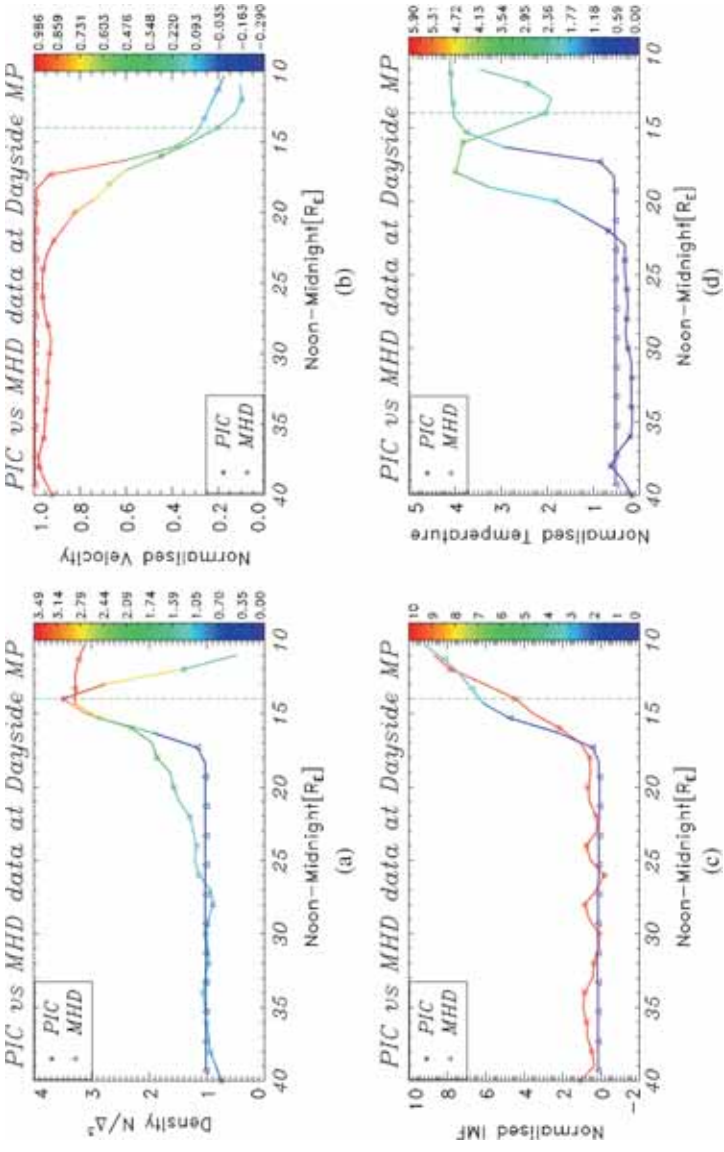

Figure 2. Colored elevated plasma parameters plotted in nose direction. (**a**) Density profile multi-plot is shown in the dayside magnetosphere as simulated by PIC code (⋆ symbol) and MHD (△ symbol). Similarly, velocity (**b**), IMF (**c**) and temperature (**d**) are depicted. All parameters are normalized to their input values. Units are in R_E.

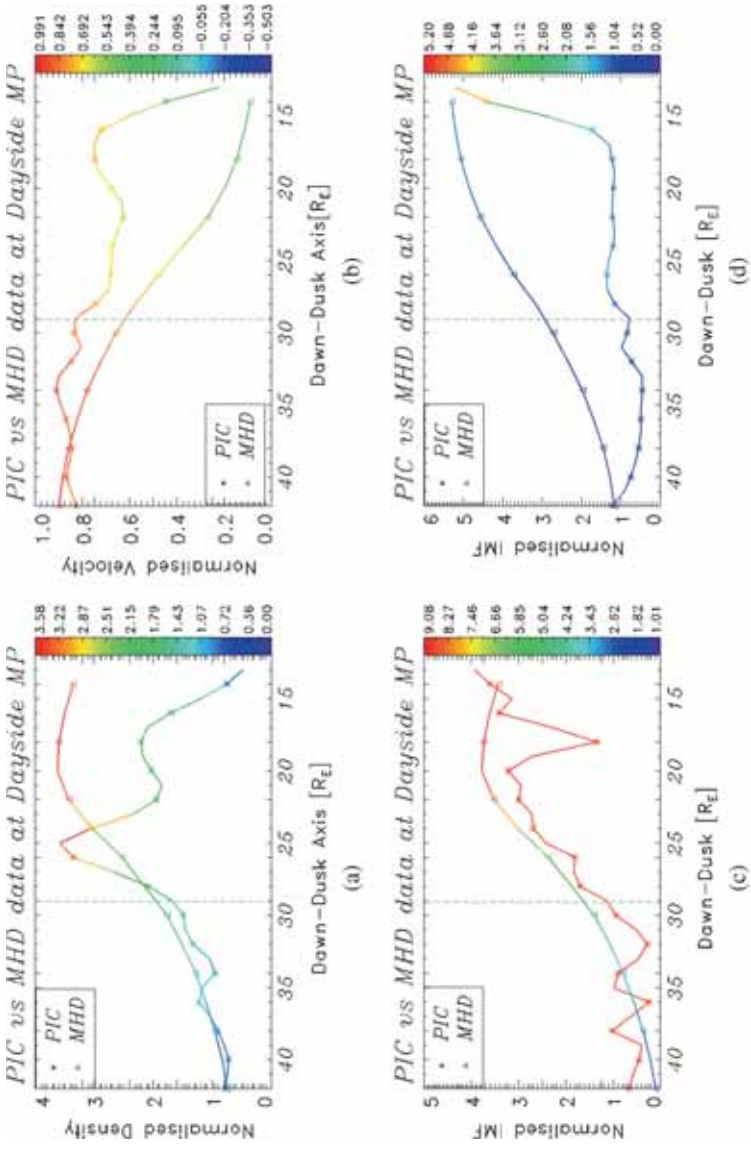

Figure 3. Colored elevated plasma parameters plotted in the dusk direction. (**a**) Density profile multi-plot is shown in the dayside magnetosphere as simulated by the PIC code (⋆ symbol) and the MHD (△ symbol). Similarly, velocity (**b**), IMF (**c**) and temperature (**d**) are depicted. All parameters are normalized to their input values. Units are in R_E.

position and shape of the Earth's bow shock as depicted in the results. The geometry of the Earth's bow shock resembles bullet-like shape (see Fig. 1). Its position was found by both codes to be equal to $14.9R_{\rm E}$ as measured along the nose direction from the planet position, and $29R_{\rm E}$ along the dusk direction. These results are in good agreement with *in situ* measurements obtained for M_A values within the range $(8-13R_{\rm E})$ (along the OX direction) as reported by Peredo *et al.* (1995), and shown in Fig. 2(a) and Fig. 3(a).

On the other hand, we see in Fig. 2(b) how the velocity simulation of both codes decreases and stagnates at the bow shock position. The simulated velocity by the PIC code shows a spatial delay compared to the sharp decrease of the MHD code , seemingly caused by the effect of thermal electrons in the foreshock region (i.e. electrons velocity spatial distribution in Fig. 4(a, b). The same effect of the velocity

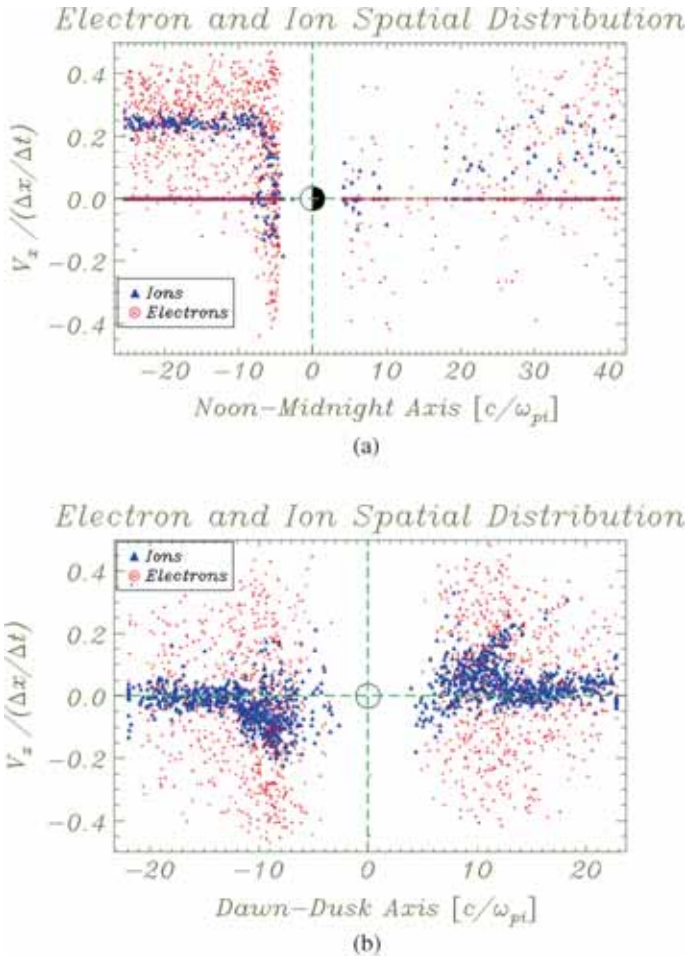

Figure 4. (**a**) Spatial distribution of ion and electron velocities taken at nose direction both in day and night side of the magnetosphere. The thermal behavior of electrons can be clearly seen in this figure, especially at the day side portion of the magnetosphere. (**b**) The spatial distribution is the same but is taken in the dusk direction.

profile of both codes can also be seen in Fig. 3(b) in the dusk side. The IMF profile along nose and dusk directions (Figures 2 and 3(c) respectively), shows similarities between both codes in the behavior of the magnetic field at the bow shock position.

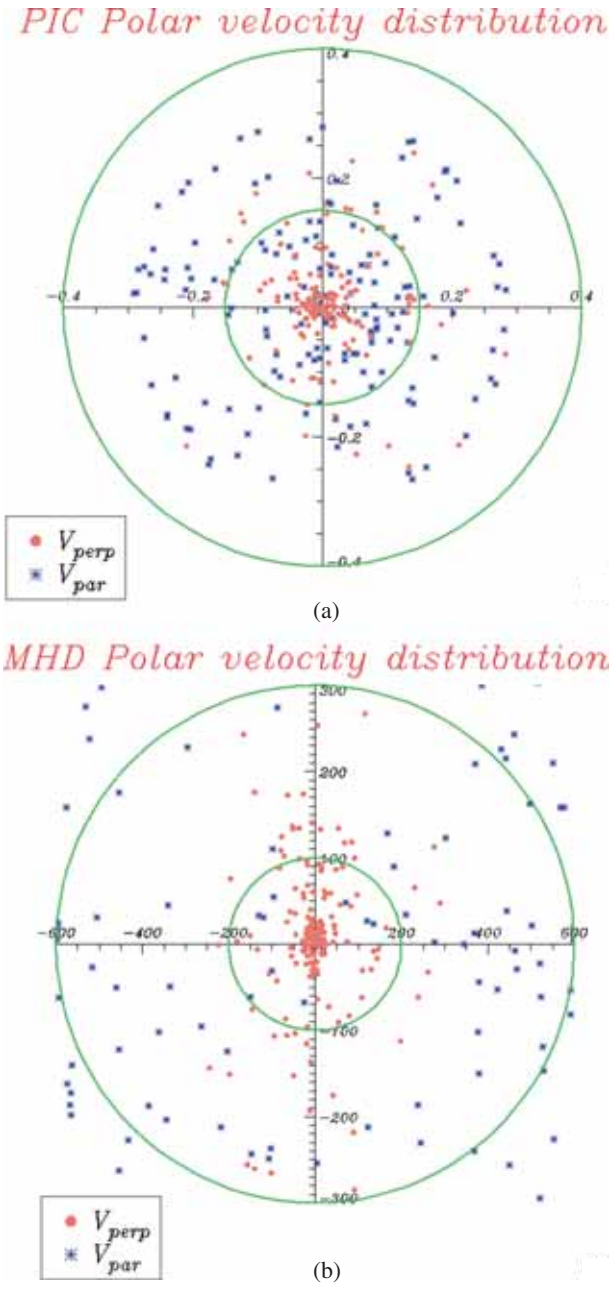

Figure 5. (**a**) The polar distribution of parallel and perpendicular velocities as generated by the PIC code (input value is $0.25 \equiv 500$ km s^{-1}). (**b**) The same distribution as simulated by MHD code (input solar wind value is 500 km s^{-1}).

Table 1. The solar wind input scaled parameters for the PIC and their corresponding values for the MHD code.

Parameters	PIC code	GUMICS-v4
CPU time	50 min	5 h
Machine	Single processor PC	CCMc super computer
Ionosphere	No	Yes
Grid cell	Fixed	Adaptive
Grid size	$1R_{\mathrm{E}}^3$	$(0.1-8R_{\mathrm{E}})^3$
Small box size	$155\times105\times105R_{\mathrm{E}}$	$250\times130\times130R_{\mathrm{E}}$
ρ	$0.8\frac{N}{\Delta^3}$	$5.0\,\mathrm{cm}^{-3}$
$B_z(x)$	0.2	6.5 (nT)
$V_x(x)$	0.25	500 (km s^{-1})
V_A	0.028	63 (km s^{-1})
	Unitless values	
$\frac{V_A}{V_{sw}}$	0.11	0.12
M_A	8.9	7.8
M_{MS}	5.5	5.2
β	1.6	2.7

On the other hand, both temperature profiles in Figures 2 and 3(d) apparently show differences and spatial lags in the temperature jump. This is because in PIC code, electron temperatures are included, but not in MHD codes, additionally the thermal velocities of electrons offset their smaller masses.

To further show similarities and differences between the two codes, the parallel and perpendicular velocity distributions of the PIC code are polar-plotted in Fig. 5(a) and for MHD code in Fig. 5(b). The maximum parallel velocity distribution values is factor 3.4 than that of the perpendicular ones for the PIC code, whilst on the other hand, this ratio is factor 2 for the MHD.

On the other hand, if we base our diagnostic on the magnetosonic Mach number $M_{\mathrm{MS}} \approx 5$ in both codes (see Table 1), the above comparison shows that PIC simulation can successfully recover the traditional results of the MHD model in terms of the macrostructure of the bow shock, but at a much lower cost in computational time. Furthermore, to our diagnostic, the magnetic field (northward input) is shown quasi perpendicularly oriented where it is plotted over the plasma density in noon–midnight in Figure 6(a) and in dawn–dusk direction in Fig. 6(b).

4. Analysis and discussion

Since the early models of the magnetosphere by Chapman & Ferraro (1930) through Dungey (1962) until present, statistical, theoretical, observational and modeling have been extensively used to comprehensively resolve the magnetospheric unsolved problems.

In our case, we do not re-invent the wheel. Our code development has been considered for upgrade for so many years and is still used in terms of spatial and temporal resolutions. Additional considerations are given to handle physical instabilities and

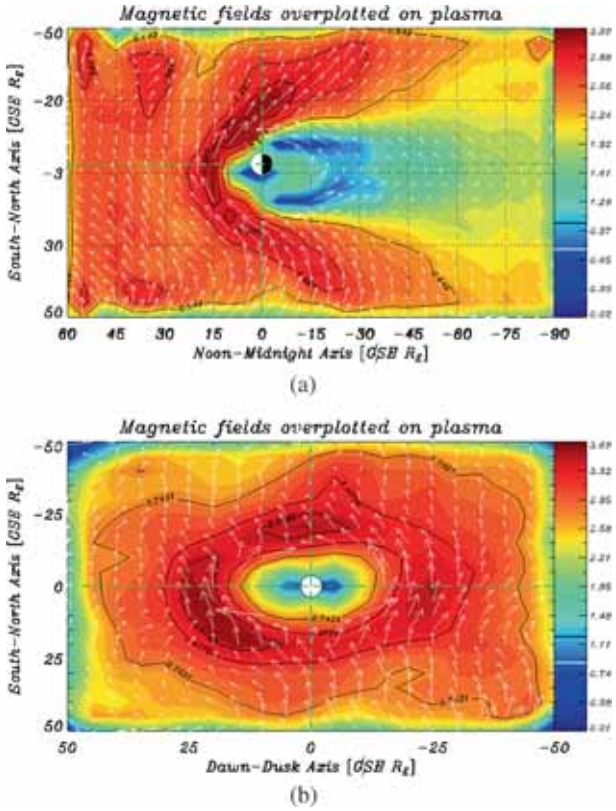

Figure 6. Vector fields in X–Z direction (**a**) are over-plotted on 2D density distribution. This figure shows field and particle updates after being run to step time $900\Delta t$. (**b**) Vector fields are plotted in Y–Z direction are over-plotted on plasma. Note the magnetic field orientation at the foreshock region in both panels.

to reduce CPU run time. In the near future, we will have a validated version of the code that is enhanced in terms of spatial and temporal resolutions with real ion to electron mass ratio. In order to keep the physical problem under investigation fixed, one has to adjust all other physical input parameters simultaneously. Because if one changes, for example, particle density to reduce statistical noises, then all other physical quantities will vary (Cai *et al.* 2003). This is exactly what has been taken care of in the current case study. The global structure of the collisionless bow shock was investigated by Omidi *et al.* (2005). In their model, ions are treated kinetically, whilst electrons are treated as a massless fluids. It is worth noting that they used 2.5D simulations, i.e., two spatial dimensions for velocity and 3D for currents. Another work consider the magnetosphere simulation by 2.5D was reported by Moritaka *et al.* (2012). They reproduced the magnetosphere. In a recent study by Cai *et al.* (2015), a large scale 3D PIC code is used to study the whole terrestrial magnetosphere using ion to electron mass ratio equal to $\frac{1}{16}$. In the current study a large scale structure of the magnetosphere was recovered but with full 3D simulations, in addition that electron kinetics are included in the run. In their simulations and ours as well, our

physical units were scaled to ion inertial lengths and all were successful in recovering the large scale magnetosphere.

However the PIC simulation is not a faithful representation of the plasma physics, it is still a must. On the other hand, even with the huge super-computing facilities available nowadays, it is quite impossible to simulate real magnetosphere. Thus scaling is an answer as quoted in the above references. After all these years and all these advances in magnetospheric physics, we still do not know the magnetosphere (private communication recently with Sitnov 2015). One can imagine a cuboid of volume of real magnetosphere equal to 1.5×10^6 Earth radii (R_E^3) which is considered for simulation while one is looking for kinetic processes that take place in few tens of meters. In this paper, a macro-structure of the Earth's magnetosphere is successfully simulated. It is quite clear that we do not have a High-Definition (HD) image with the current scaled values and their corresponding spatial and temporal resolutions, but, for global structure a little blur image is enough to give a glimpse about the considered physical problem in hand. I think if a comprehensive answer is reached in the space plasma physics field, it would have been enough for the community to pursue the discipline further. We are still on the long road to reach out there. In this section, we will analyze the criteria under which the PIC code is used in this study. The MHD code structure, boundary conditions are well defined in Janhunen *et al.* (2012). Adopting the analysis in Büchner *et al.* (2003), we simulated a dynamic system that included the bow shock in the macroscopic scale. We made sure that our total run time is very much greater than the ion gyroperiod $\tau_{\text{total}} \gg \omega_{ci}^{-1}$, where ω_{ci} is the upstream ion gyro-frequency. Typically the shock thickness is of order of few R_E, which is very much smaller than the plasma simulation box size.

In Fig. 4(a, b) we show the nose and the dusk direction respectively of ion (in blue) and electron (in red) velocities spatial distribution. In Fig. 4(a), inflow of ions have

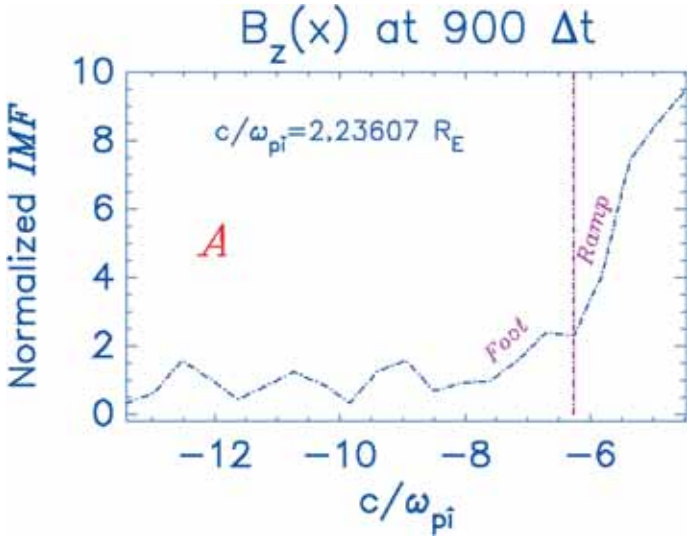

Figure 7. The $Bz(x)$ structure at the bow shock/foreshock region. $Bz(x)$ as simulated by the PIC code clearly depict the foot and ramp structure, compared with the theoretical model reported in Fig. 10 of Treumann (2009).

relatively small velocity variations before it reaches the shock terminal. Whilst on the other hand, the electron velocity in the dayside spans high variations because of their thermal motions. It is also worth noting the backstreaming of ions and electrons in the foreshock regions. The corresponding velocity spatial distributions in the dawn–dusk directions is shown in Fig. 4(b).

On the other hand, we measured the velocity (thermal) of ions in the foreshock region (at $\sim 15 R_{\mathrm{E}}$) which is found to be equal to 0.10665 (≈ 213.30 km s^{-1}) and in the magnetosheath at around $12 R_{\mathrm{E}}$ it is 0.03150 (≈ 63.0 km s^{-1}). The reference value of solar wind speed is 0.25 (≈ 500 km s^{-1}). These findings are consistent with the recent study of Pokhotelov *et al.* (2013).

Another result we report in the this paper is the magnetic field jump that was zoomed in and plotted in the foreshock region (Fig. 7) where the foot and the ramp of the shock is shown. Overshoot of the shock did not appear at this current version of the code. This result was compared with the analysis of the shock dynamics by Treumann (2009). Also we report another result here when the width of the density transition region of the shock was calculated and it was found to be ≈ 2 ion inertial lengths (c/ω_{pi}) as in Fig. 8. This result is in full agreement with Bale *et al.* (2003). This figure is mirror-imaged for comparison reason.

The width of our ramp is $1.7 c/\omega_{pi} = L_i$, which is comparable to the value $\approx 1.4 L_i$ obtained in Krasnoselskikh *et al.* (2013).

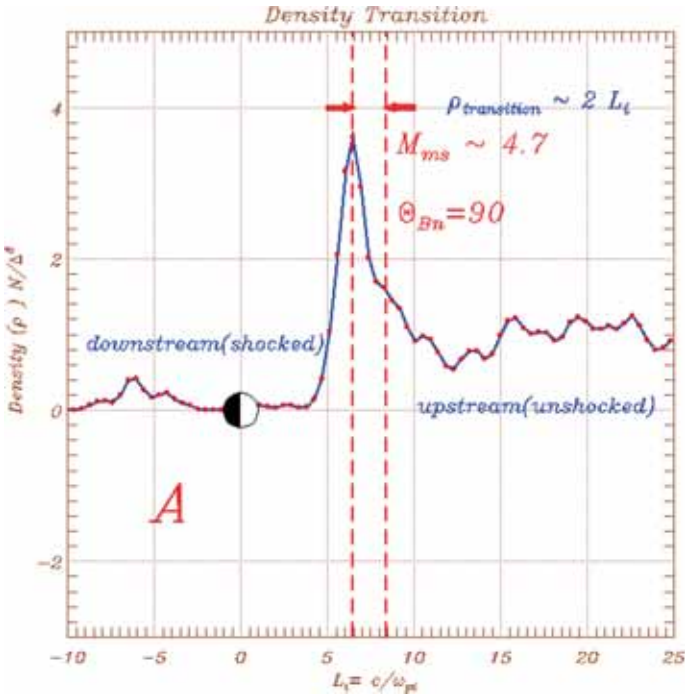

Figure 8. The density transition between downstream (shocked) and upstream (unshocked) as simulated by our code, the red vertical lines show the density transition scale. The figure is mirror imaged for comparison purposes. Our result is compared with cluster data density transition scale as reported by Fig. 5.4 of Bale *et al.* (2003).

However, it is unambiguously established that many observed thinnest ramps are less than $5c/\omega_{pi}$ thick and there was an apparent trend for lower values as $\theta_{Bn} \longrightarrow 90°$. The plasma inertia effects is considered in our PIC simulation, as a consequence, the length of the simulation box is very much larger than the Debye length $\lambda_{\mathrm{De},i} = (0.11, 0.11)$, the gyro-radius $\rho_{ce,i} = (1.25, 20)$ and the inertia lengths $\frac{c}{\omega_{pe,i}} = (5, 80)$ for electrons and ions respectively.

On the other hand, a quick look at Figure 2 ion density jump with a factor of 3, and the foot of the shock clearly appears. A time sequence study of such shocks revealed by PIC, should be carried out in a new paper for deeper verification of these preliminary results, where in Figure 2 the shock is only shown at 900 Δt.

It is also worth noting that in Figure 4, the ions and electrons at the upstream of the bow shock, have high velocities, which is consistent with observation (Filbert & Kellogg 1979; Fitzenreiter *et al.* 1984).

One final point is that we can follow the motion of electrons and ions in the self-consistent **E** and/or **B** fields obtained from a solution of Maxwell's equations, with relativistic effects readily included by the use of the Lorentz equation of motion. At this level, no approximations in the basic laws of mechanics and electromagnetism is introduced, and thus the full range of collisionless plasma physics is included in such a model (Pritchett 2000) , which is the case of the current study.

5. Conclusion

The results of this study are summarized as follows:

(1) The output data of both runs are retrieved and normalized to input plasma parameters. In this paper, we show distinct features: the bow shock position , jump conditions, plasma density, and fields distributions in specific geometric configurations.
(2) Both codes have showed that the bow shock location is found to be at $\sim 14 R_{\mathrm{E}}$ along the Sun–Earth line and at $\sim 29 R_{\mathrm{E}}$ along the dawn–dusk direction, with a factor 3 in density jump. This result is consistent with *in situ* observations obtained during similar SW and IMF conditions.
(3) The (thermal) velocity of ions in the foreshock region (at $\sim 15 R_{\mathrm{E}}$) is measured and found to be 0.10665 ($\approx$213.30 km s^{-1}) and its value in the magnetosheath at around $12 R_{\mathrm{E}}$ is 0.03150 ($\approx$63.0 km s^{-1}), the reference value of solar wind speed is 0.25 ($\approx$500 km s^{-1}).
(4) The structure of the magnetic field jump at the shock $B_z(x)$ of the foot and ramp of the magnetic field is obtained by the PIC code. The width of our ramp is $1.7c/\omega_{pi} = L_i$ which is comparable to the value of $\approx 1.4 L_i$ (Krasnoselskikh *et al.* 2013).
(5) The density transition between the shocked plasma in the downstream and the unshocked plasma in the upstream is found to be ≈ 2 ion inertial length (c/ω_{pi}) at the magnetosonic number 4.7 when $\Theta_{Bn} = 90°$.
(6) Both simulations reproduce the same basic macroscopic features of the Earth's magnetosphere. However, for the PIC code, a noisy current-sheet naturally appears, but it is absent in the MHD results.

(7) The velocity distribution of different species across and parallel to the ambient magnetic field can be derived anywhere in the magnetosphere from the PIC simulation. The derivation of that velocity distribution is also absent in MHD results.
(8) In PIC models one can follow the motion of electrons and ions in the self-consistent **E** and/or **B** fields obtained from the solution of Maxwell's equations, with relativistic effects readily included by the use of the Lorentz equation of motion.
(9) In contrast, macroscopic properties of the magnetosphere obtained from MHD simulations can be directly compared to observations, while only scaled quantities from PIC simulations are useful in such comparisons.
(10) The results obtained thus far from the present study strongly suggest using MHD and PIC codes in a complementary manner as a new strategy for better understanding of the magnetosphere-solar wind system.
(11) The PIC showed the backstreaming velocity distribution of both ions and electrons on the nose and on the dusk-direction in the dayside magnetosphere (foreshock, transition shock, magnetosheath and in the magnetotail).
(12) This working version of our PIC code is powerful to simulate large scale magnetospheric electrodynamics. It is undoubtedly capable of simulating more sophisticated kinetics, such as reconnection, cusp dynamics and current systems if and only if better computer resources and multiprocessors super computing facilities are available, in order to be able to reduce grid cell size and to increase the number of pair particles of the simulation box.

6. Future and ongoing research

(1) Magnetosphere–ionosphere coupling (code validated and tested).
(2) Simulation of plasmasphere (papers under preparation).
(3) Simulate day–night, summer–winter asymmetry of the magnetosphere.
(4) Include chemical reaction of species and exchange of charges in magnetosphere–ionosphere coupling.
(5) Ionospheric ions outflow as a function of altitude upward to magnetosphere.

Acknowledgements

This work would have not been done without the insights and hard work on code development by Dr Lotfi Ben-Jaffel, IAP. The author would also like to thank the IAP-CNRS (Paris, France), David Sibeck of NGFC-NASA, Bob Clauer of VT and Douglas Staley, President of NIA for their continuous support and insights, and Zamala program and Bank of Palestine for supporting his research visits to the US.

References

Axford, W. 1962, *J. Geophys. Res.*, **67**, 3791.
Bale, S., Mozer, F., Horbury, T. 2003, *Phys. Rev. Lett.*, **91**, 265004.
Baraka, S. 2007, Ph.D. thesis, Université Pierre et Marie Curie-Paris VI.

Baraka, S., Ben-Jaffel, L. 2007, *J. Geophys. Res. (Space Phys.)*, **112**, 6212.
Baraka, S., Ben-Jaffel, L. 2011, *Annales Geophysicae*, **29**, 31.
Baraka, S., Jaffel, L. 2014, in: AGU Fall Meeting Abstracts, Vol. 1, 4222.
Baraka, S., Jaffel, L., Dandouras, I. 2013, in: AGU Fall Meeting Abstracts, Vol. 1, 2236.
Ben-Jaffel, L., Ballester, G. E. 2014, *Astrophys. J. Lett.*, **785**, L30.
Ben-Jaffel, L., Strumik, M., Ratkiewicz, R., Grygorczuk, J. 2013, *APJ*, **779**, 130.
Birdsall, C. K., Langdon, A. B. 2005, Plasma Physics via Computer Simulaition (CRC Press).
Bonifazi, C., Moreno, G. 1981, *J. Geophys. Res.: Space Phys., (1978–2012)*, **86**, 4405.
Buneman, O. 1993, *Simulation Techniques and Software*, 67.
Buneman, O., Barnes, C., Green, J., Nielsen, D. 1980, *J. Comput. Phys.*, **38**, 1.
Buneman, O., Neubert, T., Nishikawa, K.-I. 1992, *Plasma Science, IEEE Trans.*, **20**, 810.
Buneman, O., Nishikawa, K.-I., Neubert, T. 1995, *Space Plasmas: Coupling Between Small and Medium Scale Processes*, 347.
Bykov, A., Treumann, R. 2011, *Astron. Astrophys. Rev.*, **19**, 1.
Büchner, J., Dum, C., Scholer, M. 2003, Space plasma simulation, Vol. 615 (Springer).
Cai, D., Esmaeili, A., Lembège, B., Nishikawa, K.-I. 2015, *J. Geophys. Res.: Space Phys.*, **120**, 8368.
Cai, D., Li, Y., Nishikawa, K.-I. *et al.* 2003, in: Space Plasma Simulation (Springer), 25–53.
Cai, D., Yan, X., Nishikawa, K.-I., Lembège, B. 2006, *Geophys. Res. Lett.*, 33.
Chapman, S., Ferraro, V. C. A. 1930, *Nature*, **126**, 129.
Dmitriev, A., Chao, J., Wu, D. 2003, *J. Geophys. Res.*, **108**, 1464.
Dungey, J. 1962, *J. Physical Soc. Japan Suppl.*, **17**, 15.
Ellison, D. C., Giacalone, J., Burgess, D., Schwartz, S. 1993, *J. Geophys. Res.: Space Phys. (1978–2012)*, **98**, 21085.
Filbert, P. C., Kellogg, P. J. 1979, *J. Geophys. Res.*, **84**, 1369.
Fitzenreiter, R. J., Klimas, A. J., Scudder, J. D. 1984, *GRL*, **11**, 496.
Fontaine, D., Turc, L., Savoini, P. 2015, in; EGU General Assembly Conference Abstracts, Vol. 17, 5908.
Gombosi, T., Zeeuw, D. D., Groth, C. 2000, *IEEE Trans. Plasma Sci.*
Janhunen, P., Palmroth, M., Laitinen, T. *et al.* 2012, *J. Atmos. Solar-Terrestrial Phys.*, **80**, 48.
Jelínek, K., Němeček, Z., Šafránková, J. *et al.* 2010, *J. Geophys. Res. (Space Phys.)*, **115**, 10203.
Keika, K., Nakamura, R., Baumjohann, W. *et al.* 2009, *J. Geophys. Res. (Space Phys.)*, 114.
Kellogg, P. J. 1962, *J. Geophys. Res.*, **67**, 3805.
Kowal, G., Dal Pino, E. d. G., Lazarian, A. 2011, *AJ*, **735**, 102.
Krasnoselskikh, V., Balikhin, M., Walker, S. N. *et al.* 2013, *Space Sci. Rev.*, **178**, 535.
Kronberg, E., Bučík, R., Haaland, S. *et al.* 2011, *J. Geophys. Res.: Space Phys. (1978–2012)*, 116.
Kullen, A., Janhunen, P. *et al.* 2004, in: *Ann. Geophys.*, Vol. 22, 951–970.
Leboeuf, J., Tajima, T., Kennel, C. F., Dawson, J. 1978, *Geophys. Res. Lett.*, **5**, 609.
Lindman, E. 1975, *J. Comput. Phys.*, **18**, 66.
Mann, I., Milling, D., Rae, I. *et al.* 2008, *Space Science Reviews*, **141**, 413.
Maynard, N. C., Farrugia, C. J., Burke, W. J. *et al.* 2011, *J. Geophys. Res.: Space Phys. (1978–2012)*, 116.
Meziane, K., Hamza, A. M., Maksimovic, M., Alrefay, T. Y. 2015, *J. Geophys. Res.: Space Phys.*, **120**, 1229.
Meziane, K., Wilber, M., Hamza, A. *et al.* 2007, *J. Geophys. Res.*, **112**, A01101.
Moritaka, T., Kajimura, Y., Usui, H. *et al.* 2012, *Phys. Plasmas (1994–present)*, **19**, 032111.

Nishikawa, K.-I. 1997, *J. Geophys. Res.: Space Phys. (1978–2012)*, **102**, 17631.
Omidi, N., Blanco-Cano, X., Russell, C. 2005, *J. Geophys. Res.: Space Phys. (1978–2012)*, 110.
Omidi, N., Sibeck, D., Blanco-Cano, X. *et al.* 2013, *J. Geophys. Res.: Space Phys.*, **118**, 823.
Palmroth, M., Janhunen, P., Pulkkinen, T. *et al.* 2005, in: *Annales Geophysicae*, Vol. 23 (Copernicus GmbH), 2051–2068.
Palmroth, M., Pulkkinen, T., Janhunen, P., Wu, C.-C. 2002, *J. Geophys. Res.*, **108**, SMP24.
Parks, G. K. 2004, *Space Science Reviews*, **113**, 97.
Paschmann, G., Sckopke, N., Papamastorakis, I. *et al.* 1981, *J. Geophys. Res.: Space Phys. (1978–2012)*, **86**, 4355.
Peredo, M., Slavin, J., Mazur, E., Curtis, S. 1995, *J. Geophys. Res.: Space Phys. (1978–2012)*, **100**, 7907.
Petrukovich, A., Artemyev, A., Vasko, I., Nakamura, R., Zelenyi, L. 2015, *Space Science Reviews*, **188**, 311.
Pokhotelov, D., von Alfthan, S., Kempf, Y. *et al.* 2013, in: *Annales Geophysicae*, Vol. 31 (Copernicus GmbH), 2207–2212.
Pritchett, P. L. 2000, *Plasma Science, IEEE Trans.*, **28**, 1976.
Rojas-Castillo, D., Blanco-Cano, X., Kajdič, P., Omidi, N. 2013, *J. Geophys. Res.: Space Phys.*
Samsonov, A. A. 2007, *Geomagnetism and Aeronomy*, **47**, 316.
Savoini, P., Lembege, B., Stienlet, J. 2013, *J. Geophys. Res. (Space Phys.)*, **118**, 1132.
Schreiner, C., Spanier, F. 2014, *Comput. Phys. Commun.*
Seki, Y., Nishino, M., Fujimoto, M. *et al.* 2009, *J. Geophys. Res.: Space Phys. (1978–2012)*, 114.
Shaikhislamov, I., Antonov, V., Zakharov, Y. P. *et al.* 2011, arXiv preprint arXiv:1110.4461.
Sitnov, M. 2015, private communication.
Treumann, R. 2009, *A&A Review*, **17**, 409.
Vapirev, A., Lapenta, G., Divin, A. *et al.* 2013, *J. Geophys. Res.: Space Phys.*
Villasenor, J., Buneman, O. 1992, *Comput. Phys. Commun.*, **69**, 306.
Welling, D., Liemohn, M., Toth, G., Glocer, A. 2013, in: AGU Fall Meeting Abstracts, Vol. 1, 2105.
Winglee, R., Lewis, W., Lu, G. 2005, *J. Geophys. Res.: Space Phys. (1978–2012)*, 110.
Wodnicka, E. 2009, in: *Annales Geophysicae*, Vol. 27 (Copernicus GmbH), 2331–2339.